A dCas9/CRISPR-based targeting system identifies a central role for Ctf19 in kinetochore-derived suppression of meiotic recombination

Lisa-Marie Kuhl [1], Vasso Makrantoni [2], Sarah Recknagel [1], Animish N. Vaze [1], Adele L. Marston [2] and Gerben Vader [1,3,*]

[1] Department of Mechanistic Cell Biology, Max Planck Institute of Molecular Physiology, Otto-Hahn-Strasse 11, 44227 Dortmund, Germany

[2] The Wellcome Centre for Cell Biology, Institute of Cell Biology, School of Biological Sciences, University of Edinburgh, Edinburgh, UK

[3] International Max Planck Research School (IMPRS) in Chemical and Molecular Biology, Max Planck Institute of Molecular Physiology, Otto-Hahn-Strasse 11, 44227, Dortmund, Germany

[*] correspondence: gerben.vader@mpi-dortmund.mpg.de

ORCID: G.V.: 0000-0001-5729-0991

V.M.: 0000-0003-0668-6157

A.L.M.: 0000-0002-3596-9407

Abstract

In meiosis, crossover formation between homologous chromosomes is essential for faithful segregation. However, improperly controlled or placed meiotic recombination can have catastrophic consequences on genome stability. Specifically, within centromeres and surrounding regions (*i.e.* pericentromeres), crossovers are associated with chromosome missegregation and developmental aneuploidy. In organisms ranging from yeast to humans, crossovers are repressed within (peri)centromeric regions. We previously identified a key role for the multi-subunit, kinetochore-associated Ctf19 complex (Ctf19c; the budding yeast equivalent of the human CCAN) in regulating pericentromeric crossover formation. Here, we develop a dCas9/CRISPR-based system that allows ectopic targeting of Ctf19c-subunits to a non-centromeric locus during meiosis. Using this approach, we query sufficiency in meiotic crossover suppression, and identify Ctf19 (the budding yeast homologue of vertebrate CENP-P) as a central mediator of kinetochore-associated crossover control. We show that the effect of Ctf19 is encoded in its NH_2-terminal tail, and depends on residues known to be important for the recruitment of the Scc2-Scc4 cohesin regulator to kinetochores. We thus reveal a crucial determinant that links kinetochores to meiotic recombinational control. This work provides insight into localized control of meiotic recombination. Furthermore, our approach establishes a dCas9/CRISPR-based experimental platform that can be utilized to investigate and locally manipulate meiotic crossover control. This platform can easily be adapted in order to investigate other aspects of localized chromosome biology.

Introduction

Faithful chromosome segregation in meiosis requires physical connections between initially unpaired homologous chromosomes (Petronczki, et al., 2003). Such linkages are established through homologous recombination (HR) mediated repair of programmed DNA double strand breaks (DSBs) (Keeney, 2001). Sequences that can act as HR repair templates for DSB lesions can be found on the sister chromatid and the homologous chromosome, but only repair that uses the homologous chromosome as a template can result in the reciprocal exchange of flanking chromosomal arm regions of homologous chromosomes, yielding a crossover. A crossover, together with cohesin that is laid down distally to the recombination site, establishes the connection between homologs required for successful chromosome segregation in meiosis. The placement of crossovers is determined by the location of DSB activity and by repair decisions after DSB formation. Certain regions in the genome represent a high risk to genome stability when faced with DSB repair or CO formation, and molecular systems are in place to spatially control CO placement and thereby guard genomic stability during meiosis.

Centromeres are the regions of the chromosomes where kinetochores are nucleated. Kinetochores are large multi-subunit chromatin-associated assemblies that coordinate microtubule-chromosome attachments, cell cycle control and local chromosome organization (Musacchio & Desai, 2017). DSB activity and crossover formation in centromere-proximal regions (*i.e.* pericentromeres) are suppressed in organisms ranging from yeast to human (Blitzblau et al., 2007, Borde et al., 1999, Buhler et al., 2007, Centola & Carbon, 1994, Copenhaver et al., 1999, Ellermeier et al., 2010, Gerton et al., 2000, Gore et al., 2009, Lambie & Roeder, 1988, Mahtani & Willard, 1998, Nakaseko et al., 1986, Pan et al., 2011, Puechberty et al., 1999, Saintenac et al., 2009, Westphal & Reuter, 2002). Improper placement of crossovers in pericentromeres is associated with chromosome missegregation and aneuploidy (Hassold & Hunt, 2001, Koehler et al., 1996, Lamb et al., 2005, Rockmill et al., 2006). The identity of pericentromeric sequences

and chromatin diverges widely among different organisms. In many organisms, pericentromeres are made up of heterochromatin, and the establishment of this specialized chromatin is important for the suppression of meiotic DNA break formation and recombination (Ellermeier et al., 2010). We previously identified a functional contribution of budding yeast kinetochores to local suppression of crossover formation in nearby pericentromeric sequences (Vincenten, Kuhl et al., 2015). Within budding yeast kinetochores, the Ctf19c, which is the functional and molecular equivalent of the human constitutive centromere-associated network (CCAN) (Cheeseman & Desai, 2008), plays a dual role in minimising CO formation: Ctf19c *i)* suppresses meiotic DSB formation surrounding kinetochores, and *ii)* channels the repair of remaining DSBs into intersister-directed repair. Together, these pathways lead to effective suppression of CO formation within pericentromeres (Kuhl & Vader, 2019, Vincenten et al., 2015). Our experiments identified a crucial role for pericentromeric cohesin-complexes (containing the meiosis-specific kleisin Rec8) in promoting intersister-mediated repair without affecting DSB activity (Vincenten et al., 2015). A recent study in fission yeast also identified a role for pericentromeric cohesin complexes in suppressing meiotic CO formation, although in this case the effect involved active suppression of local DSB activity (Nambiar & Smith, 2018).

Kinetochores are cooperative assemblies of several protein subcomplexes (Musacchio & Desai, 2017). This biochemical characteristic can lead to pleiotropic loss of several kinetochore subunits upon experimental interference with single components. For example, many Ctf19c subunits are co-dependent for their localization to the centromere (Lang et al., 2018, Pekgoz Altunkaya et al., 2016, Pot et al., 2003). This behaviour has complicated delineating individual contributions of single kinetochore components to specific functional pathways, including the regulation of local crossover suppression. In order to dissect individual contributions of kinetochore factors to the regulation of meiotic recombination, we developed a system that allows investigation of individual roles of kinetochore subunits in directing meiotic chromosome fragmentation and

repair, by employing the dCas9/CRISPR system. Using this approach, we identify the Ctf19 subunit of the Ctf19c as a key mediator of kinetochore-driven CO suppression. Previous work identified a key role for the unstructured NH_2-terminal region of Ctf19 in mediating recruitment of the Scc2-Scc4 cohesin regulator (Hinshaw et al., 2017, Hinshaw et al., 2015). We show that, remarkably, this 30 amino acid-region of Ctf19 is sufficient to reduce CO formation at an ectopic site, suggesting a role for local regulation of cohesin function in influencing CO positioning.

Materials and Methods

Yeast strains and growth

All strains used were of the SK1 background and genotypes are given in Supplementary Table 1. Yeast cells were grown as described in (Vincenten et al., 2015). Induction of synchronous meiosis was performed as described in (Vader et al., 2011). Synchronous entry of cultures into the meiotic program was confirmed by flow cytometry-based DNA content analysis (see below). For expression of 3xFlag-dCas9 in meiosis, Gibson assembly was used to clone *3XFLAG-dCas9-tCYC1* in a *TRP1* integrative plasmid containing the promotor of the meiosis-specific gene *HOP1* (*pHOP1*; SGD coordinates 226,101-226,601; Chr. *IX)* to create *pHOP1-3XFLAG-dCas9-tCYC1*. The plasmid containing *3XFLAG-dCas9/pTEF1p-tCYC1* was a gift from Hodaka Fujii and obtained via Addgene.org (Addgene plasmid #62190) (Fujita et al., 2018). Constructs that express different kinetochore subunits (*i.e*. *CTF19, IML3, WIP1, CTF3,* and *NDC10*) were constructed by Gibson assembly. Yeast ORFs were PCR amplified from genomic (SK1) yeast DNA. All fusion constructs were cloned in the same order: *pHOP1-ORF-3xFLAG-dCAS9-tCYC1*. *DBF4* (PCR amplified from SK1 genomic DNA) was cloned COOH-terminally of *dCAS9*, and the two ORFs were separated by a 6xGlycine linker peptide. Constructs containing $ctf19_{1\text{-}30}$, $ctf19_{1\text{-}30(2x)}$, *ctf19-9a* and $ctf19_{1\text{-}30\ 9A}$ were generated by Gibson assembly based on gene fragments synthesized by Genewiz. The two $ctf19_{1\text{-}30}$ fragments in $ctf19_{1\text{-}30(2x)}$ are separated by a 6xGlycine linker peptide. The *ctf19-9A* is based on (Hinshaw et al., 2017), and carry the following mutations in *CTF19*: T4A, S5A, T7A, T8A, S10A, T13A, S14A, S16A and S19A). SgRNA molecules were expressed from an URA3-integrated plasmid (pT040), which was a gift from John Wyrick and obtained via Addgene.org (Addgene plasmid #67640) (Laughery et al., 2015). For cloning of the three different sgRNA vectors used here, custom synthesized sgRNA cassettes for 'mock', '*III*' and '*VIII*' (Genewiz) were restriction cloned into pT040, to create the

used *URA3* integrative plasmids. The used 20-mer target-specific complementary sequences (which are located directly upstream of PAM sequence) were: '*III*': 5' TCT TAT ATA CAG GAG ATG GG 3'(SGD coordinates: 209,871-209,890; Chr. *III*). '*VIII*': 5' AGA CCT TTA TAG TAC TGT TA 3'(SGD coordinates: 146,203-146,222; Chr. *VIII*). All constructs were sequence verified.

For live cell reporter assays, we used two recombination reporter loci, as described in (Vincenten et al., 2015). For the chromosome arm reporter, *pYKL050c-CFP* was integrated at the *THR1* locus; *pYKL050c-RFP* was integrated at SGD coordinates 150,521-151,070; Chr. *VIII*; *pYKL050c-GFP** was introduced at the *ARG4* locus. For the centromeric reporter locus, *pYKL050c-CFP* was integrated at the *THR1* locus; *pYKL050c-RFP* was integrated at *CEN8* (Chr. *VIII*); and *pYKL050c-GFP** was introduced at SGD coordinates 115,024-115,582 (Chr. *VIII*). Plasmids containing *pYKL050c-CFP/RFP/GFP** were described in (Thacker et al., 2011).

To generate SK1 strains carrying *ctf19-9A* alleles, haploid strain yAM3563 (carrying *ctf19Δ::KanMX6)* was transformed with PCR product amplified from plasmid AMp1619 and corresponding to full-length *ctf19-9A* (carrying mutations: T4A, S5A, T7A, T8A, S10A, T13A, S14A, S16A and S19A as previously described (Hinshaw et al., 2017) and a downstream marker (*LEU2*). G418-sensitive, leucine prototrophs carrying all mutations were confirmed by sequencing.

Growth conditions

Solid and liquid yeast cultures were grown as described in (Vincenten et al., 2015).

SDS-Page and western blotting

Samples taken from synchronous meiotic cultures (5 mL; time points are indicted per experiments) were centrifuged at 2,700 rpm for 3 minutes. Cell pellets were precipitated in 5 mL

158 5 % TCA and washed with 800 μL acetone. Precipitates were dried overnight and resuspended
159 in 200 μL protein breakage buffer (4 mL TE buffer, 20 μL 1M DTT). 0.3 g glass beads were
160 added and the cells in the samples were lysed using a FastPrep-24 (MP Biomedicals). 100 μL of
161 3x SDS loading buffer was added, and processed using standard SDS-Page western blotting
162 methodology. The following primary antibodies were used: α-Flag M2 (Sigma-Aldrich; 1:1000),
163 α-Flag (Abcam, 1:1000) α-HA (Biolegend; 1:500, or Sigma-Aldrich; 1:1000), α-Pgk1 (Thermo
164 Fischer; 1:1000), α-GFP (Roche; 1:1000).
165
166 **Co-Immunoprecipitation**
167 Samples taken from synchronous meiotic cultures (200 mL; samples were taken 5 hours
168 post inoculation) were centrifuged at 2,700 rpm for 3 minutes. Samples were resuspended in
169 500 μL M2 buffer (0.05 M Tris (pH 7.4), 0.15 M NaCl, 1% (v/v) Triton X-100, 1 mM EDTA)
170 containing Phenylmethylsulphonylfluoride, Sodium Orthovanadate, cOmplete Mini, EDTA free
171 Protease Inhibitor Cocktail (Roche) and a protease inhibitor mix in DMSO (SERVA). 0.6 g of
172 glass beads were added and the cells were lysed in a FastPrep-24 (MP Biomedicals). Lysates
173 were sonicated using a BioruptorPlus (Diagenode) at 4 °C (set at 25 cycles of 25 seconds). Lysates
174 were centrifuged at 15,000 rpm (at 4 °C for 15 minutes). 450 μL of the cleared lysates were
175 incubated with 1 μL of primary antibody (α-Flag M2 (Sigma-Aldrich; 1:400)) at 4 °C for 3
176 hours. 25 μL of Protein G Dynabeads (Invitrogen-Thermo Fischer) was added and the samples
177 were incubated at 4 °C overnight. Resin was washed five times with 500 μL cold M2 buffer
178 and once with 500 μL cold M2 buffer without detergent. 50 μL of 2x SDS buffer was added
179 and samples were heated at 65 °C for 30 minutes. For input, 50 μL of the clear supernatant was
180 precipitated with 5 μL 100% TCA and washed with acetone. Precipitates were resuspended in
181 50 μL TCA resuspension buffer (7 M Urea, 2% SDS, 50 mM Tris (pH 7.5)), and 25 μL of 3x

182 SDS loading buffer were added. Samples were processed using standard SDS-Page western
183 blotting methodology.
184
185 **Flow cytometry**
186 Synchronous progression of meiotic cultures was assessed by flow cytometry as
187 described in (Vader et al., 2011), using an Accuri™ C6 Flow Cytometer (BD Biosciences).
188
189 **Fluorescent Crossover Reporter Assay**
190 Diploid yeast strains carrying the fluorescent reporter construct were induced into
191 synchronous meiotic liquid cultures. After 24 hours of incubation, 2 mL aliquots of those
192 samples were lightly sonicated with a Sonifier 450 (Branson Ultrasonics Corporation) (tetrad
193 integrity was not disrupted by sonication), spun down for 5 minutes at 4000 rpm in and
194 resuspended in 200 μL H_2O, and mounted onto coverslides. Imaging was done using a Delta
195 Vision Ultra High Resolution Microscope (GE Healthcare), whereby each chosen coordinates of
196 the sample were imaged in the CFP, mCherry and Green channel. The pictures were processed
197 with ImageJ. Only tetrads comprising four visible spores in the CFP channel were counted, in
198 order to prevent confounding effects due to meiotic chromosome missegregation. Map distance
199 (cM) and standard errors were calculated using online tools
200 (http://elizabethhousworth.com/StahlLabOnlineTools/EquationsMapDistance.html) . Statistical
201 significance was calculated using Fisher's exact test
202 (https://www.socscistatistics.com/tests/fisher/default2.aspx).
203
204 **Chromatin immunoprecipitation**
205 Cells of 100 ml sporulation culture (harvested 4.5 hours post inoculation) were
206 crosslinked with 1% formaldehyde for 15 min at room temperature. Crosslinking was quenched

for 5 min at room temperature by adding 2.5 M Glycine to a final concentration of 125 mM. Quenched cells were pelleted for 3 min at 4 °C, at 3,000 rpm and washed once with 20 mL ice-cold 1x TBS buffer. Pre-chilled M2 lysis buffer and an equal volume of glass beads (Carl Roth) was added. Cells were lysed using a FastPrep-24 (MP Biomedicals). Cell lysates were mixed on a VXR basic Vibrax (IKA) for 2 min at 1500 rpm. Chromatin was fragmented by sonication using Branson Sonifier 450 at output control 2, constant cycle three times for 15 sec. In between runs, samples were kept on ice for 2 min. Cellular debris was pelleted for 10 min at 4 °C, 15,000 rpm and crude lysate was collected. As input sample, 50 µL of the crude lysate was added to 200 µl of 1x TE/ 1% SDS buffer and stored at 4 °C until reversal of crosslinking. For α-Flag ChIPs, 500 µL of the crude lysate was incubated with 40 µL of 50 % slurry of α-Flag M2 beads (Sigma-Aldrich) for 2 hours, after which resin was washed four times with 500 µL of ice-cold M2 buffer and once with 500 µL of M2 buffer without detergent. Protein-DNA complexes were eluted from the beads by adding 200 µL of ice-cold M2 buffer without detergent containing 3xFLAG peptides (Sigma-Aldrich) (final concentration of 150 ng/µL) and rotated at 4 °C for 30 min. Resin was pelleted in a refrigerated centrifuge for 30 sec at 9,000 rpm and the supernatant containing the protein-DNA complexes was transferred to a new tube. This step was repeated and 800 µL of 1x TE/ 1% SDS buffer was added to the total eluate. For α-HA ChIPs, 500 µL of the crude lysate was incubated with 1µL of α-HA antibody (BioLegend) for 3 hours at 4 °C. 35 µL of a 50% slurry of protein G Dynabeads (Invitrogen) was added, and lysate was incubated overnight at 4 °C. Resin was washed four times with ice-cold M2 buffer without inhibitor, and once with ice-cold M2 buffer without detergent. Supernatant was removed, and resin was resuspended in 200 µL of 1x TE/ 1% SDS buffer and incubated at 65 °C for 18 hours to reverse crosslinking. 5 µL of glycogen (20 mg/ ml) and 5 µl of proteinase K (20 mg/ ml; Roche) were added to the samples and incubated at 37 °C for 2 hours. ChIP samples

were split and 68.7 µL of 3 M LiCl and 1 mL of 100% ethanol was added to the input and ChIP samples and precipitated at – 20 °C overnight. DNA was pelleted at 15,000 rpm for 10 min and washed once with 75% ethanol. DNA pellets were resuspended in 50 µL of TE containing RNAse A (1 µL / 100 µL) and incubated at 37 °C for 30 min. Real time quantitative PCR (qPCR) was performed using a 7500 Fast Real-Time PCR System (Applied Biosystems). PerfeCTa® SYBR® Green FastMix was used. The threshold cycle number (C_t value) of a fast 2-Step cycling program for product detection was used to normalize the ChIP-qPCR data according to the Percent Input method.

Primers used:

GV2464: 5' CGT AGA TTT TAT ACA CGC AC 3'

GV2465: 5' GAG GCA GGT CTA AGA AGA AA 3'; primer pair amplifies SGD coordinates 209,845-209,921; Chr. *III*.

GV2472: 5' TAAATGTACCTTACCATGTTG 3'

GV2473: 5' TCCGGACTCGTCCAATCTTT 3'; primer pair amplifies SGD coordinates 146,165-146,236; Chr. *VIII*.

GV2569: 5' GATCAGCGCCAAACAATATGGAAAATCC 3'

GV2570: 5' AACTTCCACCAGTAAACGTTTCATATATCC 3'; primer pair amplifies SGD coordinates 114,321-114,535; Chr. *III*.

Southern blot analysis of DSB formation.

Southern blotting was performed as previously described (Vader et al., 2011), using the following probe (SGD coordinates): *YCR047C*; *III*, 209,361-201,030; Chr. *III*. DSB intensities were calculated from three independent experiments using ImageJ. Error bars indicate standard error of the mean.

256 **Spo11-oligo mapping**

257 Spo11 oligo mapping data from wild type strains mapped to the S288c genome
258 assembly R64 (sacCer3) and normalized to the total number of uniquely mapped reads (reads
259 per million) was retrieved from the Gene Expression Omnibus (GEO), access number:
260 GSE67910 (GSM1657849 and GSM1657850) (Zhu & Keeney, 2015). Peaks were visualized
261 on Integrative Genome Browser.

262

263

Results

To dissect individual contributions of kinetochore factors to regulation of meiotic recombination, we developed a system to query the individual roles of kinetochore (and specifically, Ctf19c) subunits in directing meiotic chromosome fragmentation and repair. We were inspired by earlier approaches, that relied on integration of ectopic DNA arrays coupled to the expression of cognate targeting units fused to genes of interest, to successfully isolate aspects of kinetochore function (Gascoigne et al., 2011, Ho et al., 2014, Kiermaier et al., 2009, Lacefield et al., 2009). However, since DNA integration can cause unwanted effects on meiotic DSB/recombination patterns, we opted for an approach not requiring integration of foreign DNA at a locus of interest. The CRISPR-dCas9 system (Wang et al., 2016) employs a mutated, catalytically-dead version of Cas9 nuclease (Gilbert et al., 2013) (dCas9) that can be recruited to genomic loci when paired with specific single guide RNAs (sgRNAs) (**Figure 1A**). sgRNA-driven recruitment of dCas9 occurs without cleavage of the targeted DNA sequence, and can direct fused proteins of interest to defined loci. This approach has successfully been used for a myriad of applications (*e.g.* (Liu et al., 2017, Xu et al., 2016)). We used a dCas9 that was tagged at its NH_2-terminus with a 3xFlag tag (3xFlag-dCas9) and placed under the control of the promoter of the meiosis-specific *HOP1* gene (*pHOP1,* creating *pHOP1-3XFLAG-dCas9*), ensuring meiosis-specific expression to avoid potential interference with chromosome segregation during vegetative growth (Vershon et al., 1992) (**Figure 1A and B**). Western blot analysis using α-Cas9 or α-Flag confirmed the meiosis-specific induction of 3xFlag-dCas9 (**Figure 1C**). We combined this system with a fluorescence-based assay to measure local CO recombination frequencies within a defined region on the (non-pericentromeric) arm of chromosome *VIII* (Thacker et al., 2011, Vincenten et al., 2015) (**Figure 1D-F**). Throughout this study we used three sgRNA expression cassettes (Laughery et al., 2015) in combination with dCas9-fusion constructs: one sgRNA targets an intergenic chromosomal position between the

genes *YHR020W* and *YHR021C* located within the 10 kilobase interval flanked by the GFP and RFP markers of the recombination reporter on chromosome *VIII* (Thacker et al., 2011) (**Figure 1D** and **Supplementary Figure 1A**). We previously observed a ~6 kb sized DSB effect surrounding centromeres (Vincenten et al., 2015), and thus chose a target position within a distance of ~2.5 kilobases from the major DNA break hotspot in the divergent promoters of the genes *YHR019C* and *YHR020W* (Pan et al., 2011). This sgRNA molecule is referred to as '*VIII*'. We also used a sgRNA ('*III*'), which directs the dCas9 to the intergenic region in between *YCR045C* and *YCR046C* on chromosome *III*, in the vicinity (~1,8 kilobases away) of a strong natural DSB hotspot ('*YCR047C*'; **Figure 6A** and see below). We further used a sgRNA molecule that lacks the 20-nt target sequence, referred to as 'mock', as a control. sgRNA *VIII* and *III* are located in intergenic regions to minimize interference with the gene expression in order to prevent potential indirect effects on DSB activity (**Figure 6** and **Supplementary Figure 1**). We performed α-Flag ChIP-qPCR to confirm specific enrichment of 3xFlag-dCas9 to desired regions when combined with the corresponding sgRNAs (**Figure 1G**). We next ascertained that targeting of 3xFlag-dCas9 within the reporter locus on chromosome *VIII* or when combined with *III* or mock sgRNAs did not interfere with wild type recombination frequencies in this interval (**Figure 1H**). Indeed, upon 3xFlag-dCas9 targeting, observed crossover frequencies were indistinguishable from reporter frequencies within this interval (*i.e.* without any dCas9 expression or targeting) (Vincenten et al., 2015). These results verify the development of our ectopic targeting system to investigate meiotic recombination, and show that dCas9 can be targeted to defined regions within the genome without causing unwanted effects on meiotic recombination frequencies.

Fusions of dCas9 with selected kinetochore components were generated, in order to interrogate contributions of these factors (and directly associated and co-targeted factors) to local suppression of meiotic recombination. We fused factors of the budding yeast kinetochore at their

COOH-termini with the 3xFlag-dCas9 moiety (*i.e.* the organization of these polypeptides is: protein of interest-3xFlag-dCas9, where the 3xFlag moiety also functions as an unstructured linker peptide). Functional COOH-terminal GFP fusions of the factors that we investigated here (see below) have been described (*e.g.* (Ho et al., 2014) (Schmitzberger et al., 2017) (Schleiffer, Maier et al., 2012), which we reasoned increased the chances that similarly organized dCas9 fusions would be functional. Five factors that represent kinetochore/Ctf19C sub-complexes within the Ctf19C were investigated: Ctf19, Iml3, Wip1, Ctf3 and Ndc10 (**Figure 2A**). All factors were efficiently expressed during meiosis when fused to 3xFlag-dCas9 (like 3xFlag-dCas9, expression of these constructs was driven by *pHOP1*) (**Figure 2B**). Importantly, Ctf19-, Iml3-, Wip1-, and Ctf3-3xFlag-dCas9 fusions were able to rescue spore viability defects normally observed in their respective gene deletions (**Supplementary Figure 2A-C**), confirming functionality of these fusion proteins. In addition, ectopic expression in an otherwise wild type background did not interfere with endogenous kinetochore function and meiotic chromosome segregation (**Supplementary Figure 2A-C**). Due to the essential nature of *NDC10*, we did not test functionality of Ndc10-3xFlag-dCas9.

We investigated whether ectopic recruitment of these factors resulted in effects on recombination frequencies on chromosome *VIII*. Interestingly, we observed a moderate, but significant reduction in recombination frequency in cells expressing Ctf19-3xFlag-dCas9 in combination with sgRNA *VIII* (**Figure 2C**). This effect appeared specific for Ctf19: targeting Iml3, Wip1, Ctf3 or Ndc10 did not significantly change frequencies. In addition, the Ctf19-driven effect depended on its local recruitment: when *pHOP1-CTF19-3XFLAG-dCAS9* was combined with mock or *III* sgRNAs, no effects on recombination frequencies on the interval on chromosome *VIII* where observed (**Figure 2D**). These data demonstrate the feasibility of our dCas9-targeting system and isolate the Ctf19 subunit of the kinetochore as a factor whose local targeting at a non-centromeric locus is able to influence meiotic recombination.

We aimed to further investigate the contribution of Ctf19 to ectopically-induced crossover regulation. Ctf19 is an RWD domain-containing protein that forms a stable heterodimer with Mcm21, also an RWD domain protein (Schmitzberger & Harrison, 2012)). Together with Ame1 and Okp1, the Ctf19-Mcm21 dimer forms the COMA Ctf19c-subcomplex (De Wulf et al., 2003) (**Figure 3A**). We found that the fusion protein Ctf19-3xFlag-dCas9 co-immunoprecipitates with Mcm21-3HA (**Figure 3B**), and, as judged by ChIP-qPCR, was able to co-recruit Mcm21-3HA to the target locus on chromosome *VIII* (**Figure 3C**). This indicates that Ctf19-Mcm21 (and possibly the entire COMA complex) is co-recruited upon targeting of Ctf19 to an ectopic location. The assembly of additional Ctf19-C proteins, such as the Chl4-Iml3 subcomplex, at kinetochores depends on COMA (Schmitzberger et al., 2017) (Pot et al., 2003). Despite an efficient interaction between Ctf19-3xFlag-dCas9 and Chl4-3HA (as judged by Co-IP; **Figure 3D**), we did not observe Chl4-3HA accumulation at the target locus on arm *VIII* in *pHOP1-CTF19-3XFLAG-DCAS9, sgRNA-VIII* expressing cells. This observation reveals that ectopic targeting of Ctf19 is not sufficient to co-recruit the Chl4-Iml3 complex (**Figure 3E and Supplementary Figure 3A**). The discrepancy between the interaction and recruitment could be explained by the observed interaction taking place at native kinetochores, where Ctf19-3xFlag-dCas9 is present, in addition to the ectopic targeting site (note that Ctf19-dCas9 rescued *ctf19Δ*, indicating that this fusion is incorporated into native kinetochores, **Supplementary Figure 2A**). We did not detect an interaction between Mtw1-GFP (a non-Ctf19C kinetochore factor) and Ctf19-3xFlag-dCas9 (**Supplementary Figure 3B**). These data demonstrate that ectopic targeting of Ctf19 leads to co-recruitment of its direct binding partner Mcm21 (and thus potentially of the entire COMA complex), but is insufficient to lead to co-recruitment of other Ctf19C/kinetochore factors, such as Iml3-Chl4 and Mtw1.

Our results suggest that the effect of Ctf19-3xFlag-dCas9 on crossover suppression is encoded within the factors that are recruited to the ectopic site. From this it follows that the Ctf19-

364 driven effect should occur independently of non-recruited kinetochore factors, such as the Chl4-
365 Iml3 complex. Indeed, targeting of Ctf19-3xFlag-dCas9 in *iml3Δ* cells to the target locus on arm
366 *VIII* led to an equal reduction in recombination rates, as in a wild type background **(Figure 3F**
367 **and G**). This points to a central role for Ctf19 (and potentially its associated COMA complex
368 binding partners, such as Mcm21) in regulating crossover suppression.

369 To dissect how Ctf19 influences meiotic recombination, we focussed on the role of Ctf19
370 in regulating cohesin (Fernius & Marston, 2009) (Hinshaw et al., 2017, Hinshaw et al.,
371 2015)(**Figure 4A**). Ctf19 recruits Scc2-Scc4, a key regulator of chromosomal loading and
372 stimulator of cohesin ATPase activity, to kinetochores and influences cohesin throughout
373 surrounding pericentromeres (Davidson et al., 2019, Fernius & Marston, 2009, Gutierrez-
374 Escribano et al., 2019, Hinshaw et al., 2017, Hinshaw et al., 2015, Petela et al., 2018). Scc2-Scc4
375 associates with the first 30 NH_2-terminal amino acids of Ctf19, and this interaction is dependent
376 on phosphorylation of 9 serine/threonine residues within this region by the Cdc7/Dbf4 kinase
377 (also known as DDK) (Hinshaw et al., 2017). Mutating these residues to non-phosphorylatable
378 residues (in the *ctf19-9A* allele) impairs efficient recruitment of Scc2-Scc4 and has downstream
379 effects on cohesin function (Hinshaw et al., 2017). We found that when targeted to the target
380 locus on arm *VIII,* Ctf19-9A was unable to suppress recombination frequencies (in fact, crossover
381 frequency was slightly increase under this condition), in contrast to what was observed for wild
382 type Ctf19 **(Figure 4B** and **C)**. Ctf19-9A was, as expected, still able to associate with Mcm21
383 and Chl4 (**Figure 4D** and **Supplementary Figure 4A**). These results suggest that the effect of
384 Ctf19 on local crossover suppression was likely connected to its described role in kinetochore-
385 recruitment of Scc2-Scc4, and downstream effects on cohesin function.
386 We aimed to further explore this idea. First, we tested the ability of a construct containing the
387 first 30 NH_2-terminal amino acids of Ctf19 (which fall outside of the structured RWD) in
388 mediating crossover reduction. Strikingly, we found that the first 30 NH_2-terminal amino acids

of Ctf19 (when fused to dCas9) were sufficient to instigate crossover suppression to the same level as full length Ctf19 (**Figure 4E-G)**. Importantly, as in the full-length case, this suppression was abolished upon mutation of the 9 DDK-targeted residues in this NH_2-terminal fragment. $Ctf19_{1-30}$ was unable to associate with Mcm21 or Chl4, as expected from the described requirement for the RWD domain of Ctf19 in mediating interactions with the COMA and Ctf19c components **(Figure 4H** and **Supplementary Figure 4B)**. These findings show that the suppression of meiotic recombination instated by Ctf19 is encoded in its NH_2-terminal tail, and depends on residues that are important for the recruitment of the Scc2-Scc4 cohesin regulator.

Although our recombination analysis established that ectopic targeting of Ctf19 causes crossover suppression, the effect that we observed at an ectopic locus was not as penetrant as (Ctf19-dependent) suppression of recombination observed at native pericentromeres (Vincenten et al., 2015). This can ostensibly be because certain aspects/factors of native kinetochores that contribute to efficient recombinational suppression might not be efficiently recapitulated in our ectopic targeting system. We aimed to address this possibility. First, we considered the stoichiometry of the native kinetochore. Based on biochemical and structural analyses, it is assumed that the kinetochore contains two Ctf19c assemblies (Hinshaw & Harrison, 2019, Yan et al., 2019)(**Figure 5A**). In our dCas9-targeting system, we only target a single Ctf19-molecule; we thus aimed to engineer a fusion construct that allowed 'dimeric' targeting of Ctf19. To do so, we made use of the fact that $Ctf19_{1-30}$ was sufficient to trigger crossover suppression. We constructed a dimeric $Ctf19_{1-30}$ ($Ctf19_{1-30(2X)}$)-dCas9 fusion (**Figure 5B**), and expression of this construct led to a stronger reduction on recombination frequency as compared to the 'monomeric' $Ctf19_{1-30}$ (**Figure 5C** and **D**). Importantly, the suppression of crossover activity in this 'dimeric' construct was present even in *mcm21Δ* cells (**Figure 5E and F**), again strengthening the conclusion that observed crossover suppression is driven by the NH_2 terminus of Ctf19, and occurs independently of the direct binding partner of Ctf19, Mcm21.

Next, we focused on Cdc7/DDK, which is recruited to kinetochores in a Ctf3-dependent manner (Hinshaw et al., 2017). DDK is responsible for the phosphorylation-dependent binding of Scc2-Scc4 to the NH_2-terminus of Ctf19 (Hinshaw et al., 2017). We surmised that Ctf3 (and thus DDK) would not be effectively co-recruited by Ctf19-dependent targeting. Under such an assumption, non-kinetochore, chromatin-associated DDK would be responsible for (potentially inefficient) phosphorylation of Ctf19. Cdc7/DDK is associated with traveling replisomes (Murakami & Keeney, 2014, Takahashi et al., 2008), and this pool of DDK could be responsible for phosphorylation of ectopically targeted Ctf19. We thus aimed to co-recruit Dbf4 (and with it Cdc7) to Ctf19. To do so, we generated a *CTF19-dCAS9-DBF4* construct, wherein Dbf4 is fused to the COOH-terminus of dCas9 (note that in this construct, dCas9 and Dbf4 are separated by an unstructured linker peptide) (**Figure 5G**). Interestingly, we observed that expressing this chimeric fusion construct led to stronger suppression of crossover frequency as compared to Ctf19-dCas9 alone (**Figure 5H** and **I**). Importantly, mutation of the nine NH_2 phosphoacceptor sites of Ctf19 in a chimeric fusion between Ctf19, dCas9 and Dbf4 (*i.e. ctf19-9A-dCAS9-DBF4*) largely eliminated crossover suppression (**Figure 5H**). These data together suggest that efficient phosphorylation of (the NH_2 terminus of) Ctf19, driven by DDK, is crucial for crossover suppression.

We aimed to investigate how ectopic targeting led to local crossover suppressive function. In our earlier work (Vincenten et al., 2015), we proposed that crossover suppression at pericentromeres is achieved by *i)* a suppression of DSBs and *ii)* a preferential channelling of remaining DSBs into the repair pathway that yields intersister CO repair over interhomolog CO repair. Ctf19 likely plays a role in both pathways (Vincenten et al., 2015), and we investigated whether ectopic targeting of Ctf19 led to local decreases in DSB activity. To test this, we used our system to recruit several Ctf19-fusion constructs to the vicinity of the *YCR047C* DSB hotspot on chromosome *III*, using sgRNA *III*. As shown in **Figure 6A-C**, the targeting of either Ctf19,

439 $Ctf19_{1\text{-}30(2X)}$, or Ctf19 together with Dbf4, did not significantly alter DSB levels, as judged by
440 Southern blot analysis of DNA breakage at *YCR047C*. This suggests that the crossover-
441 suppressive functionality that was seen in the Ctf19-based targeting modules occurs
442 independently of a DSB-reducing effect. We suggest that the DSB-protective role of
443 Ctf19/Ctf19c is related to its structural role in establishing kinetochore integrity (Pot et al., 2003)
444 (Lang et al., 2018, Pekgoz Altunkaya et al., 2016).

445 Finally, we aimed to address whether the observations made using our ectopic targeting
446 system also held true at native pericentromeres. We thus analyzed crossover frequency using a
447 live cell reporter assay to measure recombination frequency in the vicinity of *CEN8,* as described
448 earlier (Vincenten et al., 2015) in a *ctf19-9A* mutant background. Indeed, as expected from our
449 dCas9-based analysis, we found that *ctf19-9A* triggered a specific increase in crossover frequency
450 at *CEN8* **(Figure 7A)**. Together, these experiments, together with earlier work that linked
451 Scc2/Scc4 function to local crossover control (Vincenten et al., 2015), demonstrate that, also at
452 native kinetochores, the NH_2 terminus of Ctf19 is central to regulation of local crossover repair
453 of meiotic DSBs.
454

Discussion

Control of DSB formation and meiotic crossover repair is crucial for faithful execution of the meiotic program. Too few or too many crossovers, crossovers placed at the wrong location, or DSB formation within at-risk regions endanger fidelity of meiosis and jeopardize genome stability (Sasaki et al., 2010). Many factors influence crossover formation, either by influencing DSB activity or post-DSB repair decisions (Hunter, 2015, Keeney, 2001), and manipulating these factors leads to global DSB and/or recombination effects. In addition, localized systems that control recombination within specific genomic regions exist (*e.g.* (Ellermeier et al., 2010, Nambiar & Smith, 2018, Vader et al., 2011, Vincenten et al., 2015)). One such localized mechanism is kinetochore-derived and minimizes DSB activity and crossover formation within surrounding pericentromeres (Vincenten et al., 2015). Here, we shed light on this mechanism. We developed a dCas9-based system that allowed us to target individual kinetochore/Ctf19c subunits, and to precisely dissect the mechanism of kinetochore-driven crossover regulation. Using this system, we identified the Ctf19 protein as a nexus in mediating kinetochore-derived crossover suppression.

Ctf19 is an RWD-domain containing protein, whose structural role within the kinetochore is linked to its assembly into the COMA complex (together with Okp1-Mcm21-Ame1) (Schmitzberger & Harrison, 2012, Schmitzberger et al., 2017). In addition, the unstructured NH_2-terminal extension (amino acids 1-30) of Ctf19 functions as a phospho-dependent binding site for the Scc2/Scc4 cohesin loader and activator complex (Fernius & Marston, 2009, Hinshaw et al., 2017, Hinshaw et al., 2015). We provide evidence that the contribution of Ctf19 to local crossover regulation is mediated by this pathway: *i)* abolishing the DDK-driven phosphorylation (by mutating 9 phosphoacceptor sites (*ctf19-9A*)) prevents crossover suppression in a dCas9-targeted Ctf19 fusion, *ii*) the NH_2-terminal 30 amino acids ($ctf19_{1\text{-}30}$) are sufficient to mediate ectopic suppression when targeted, and suppression depends on the same phosphoacceptor sites,

480 *iii*) co-targeting Dbf4 (*i.e.* DDK) with this NH_2-terminal fragment strengthens crossover
481 suppression, in a manner that again depends on the presence of phosphorylatable residues within
482 $Ctf19_{1-30}$, and *iv)* mutating the 9 DDK phospho-sites in Ctf19 (*i.e. ctf19-9a*) leads to increased
483 crossover recombination at a native pericentromere. Taken together, our findings suggest that the
484 NH_2 region of Ctf19, through the recruitment of DDK-driven Scc2/4, impacts local crossover
485 regulation. How does this pathway eventually suppress crossover formation? Local Scc2/4
486 function can alter cohesin function, by enhancement of chromosomal loading and via stimulation
487 of cohesin's ATPase activity (and likely also cohesin-dependent loop extrusion activity) (Petela
488 et al., 2018) (Davidson et al., 2019, Fernius & Marston, 2009, Gutierrez-Escribano et al., 2019,
489 Hinshaw et al., 2017, Hinshaw et al., 2015, Paldi et al., 2019). We proposed earlier that this
490 alteration in cohesin function leads to a local shift in repair choice from interhomolog- into
491 intersister-based repair (Kim et al., 2010) (Vincenten et al., 2015). As such, local DSB repair will
492 favor the eventual repair by using sequences present on sister chromatids. Intersister-based repair
493 does not lead to crossover formation (and interhomolog connections) and has been proposed to
494 preferentially occur within pericentromeric regions (Vincenten et al., 2015). Our data thus
495 strengthen the idea that a central role of the kinetochore (and Ctf19) in minimizing meiotic
496 crossovers revolves around its influence on local cohesin function (Kuhl & Vader, 2019).

497 The level of crossover suppression that we observed upon targeting of Ctf19 was modest
498 in comparison to the crossover suppression normally seen around native kinetochores; for
499 example, compare the data in **Figures 2-5** to those in **Figure 7**; also see (Vincenten et al., 2015).
500 We envision several possible (technical and biological) explanations for this discrepancy, and
501 we addressed some of these in this study.

502 First, as we show in **Figure 6**, ectopic targeting of Ctf19 does not appear associated with local
503 DSB suppression. At native kinetochores the Ctf19c suppresses DSB activity ~5-fold within the
504 6 kb genomic regions that surround centromeres. A lack of DSB suppression in the case of

ectopic Ctf19-targeting (as observed here) can explain (in part) why total crossover repression is not as penetrant as normally seen around native kinetochores. In agreement with this interpretation (and with our results upon targeting Ctf19 and its NH_2-terminal fragments), interfering with cohesin function (via the *scc4-m35* allele) (Hinshaw et al., 2015) did not impair kinetochore-driven DSB suppression (Vincenten et al., 2015). These findings hint that DSB suppression at native kinetochores is related the structural assembly of the Ctf19c/kinetochore.

Second, it is likely that the targeting of Ctf19 using our dCas9-system fails to completely reconstitute particular aspects of kinetochore organization that influence crossover regulation. In fact, we initially set out to achieve exactly this, since such a condition would allow for dissection of functionalities. The stoichiometry of native kinetochores (each thought to contain two Ctf19c assemblies (Hinshaw & Harrison, 2019, Yan et al., 2019)) is not recapitulated in single sgRNA-based targeting, which might explain lower suppression strength. Indeed, engineering a dCas9-molecule with two Ctf19 NH_2 moieties enhanced suppression strength (**Figure 5C** and **D**), suggesting that stoichiometry of kinetochore factors is important for crossover regulation. In addition, certain regulatory aspects encoded in non-Ctf19 subunits of the kinetochore might collaborate with the 'Ctf19-pathway' in mediating crossover suppression. Indeed, it is known that DDK is recruited to native kinetochores via Ctf3, and that kinetochore-association of DDK is required for efficient phosphorylation of Ctf19 (Hinshaw et al., 2017). This aspect of kinetochore function is likely not recapitulated in Ctf19-targeted situations. Direct fusion of Dbf4 to Ctf19-dCas9 led to increased crossover suppression, likely caused by more efficient phosphorylation of Ctf19 (**Figure 5H** and **I**). Furthermore, recent work has demonstrated that pericentromeres adopt a specialized 3D confirmation, coordinately driven by local gene organization and kinetochores (Paldi et al., 2019). Pericentromeric 3D organization might play a role in local crossover regulation, and it is conceivable that the ectopic sites we study here do not

529 exhibit optimal gene organization to allow efficient formation of such a chromosome
530 architecture.
531 Third, we do not currently know the efficiency and variability of dCas9-mediated targeting in
532 individual cells. It is possible that a subpopulation of cells fails to efficiently recruit dCas9-fusion
533 constructs, which could result in less efficient overall suppression frequencies.
534 Methods that allow for specific targeting of individual components of chromosomal
535 regulatory system to ectopic sites (in isolation from native binding partners or complexes) are
536 useful tools to interrogate and dissect functional contributions (for example, see (Gascoigne et
537 al., 2011, Ho et al., 2014, Kiermaier et al., 2009, Lacefield et al., 2009)). To our knowledge, we
538 are the first to use of dCas9-technology to establish such a method, and use this approach to
539 locally manipulate crossover formation via the targeted recruitment of specific factors. The
540 method that we developed here should be readily adaptable to allow the investigation and
541 manipulation of other aspects of (meiotic and/or mitotic) chromosome biology. We note that
542 modulating crossover frequencies is a major engineering goal in crop development (Choi, 2017,
543 et al., 2017). Our approach could provide a basis to explore local manipulation of meiotic
544 recombination in plant breeding while eliminating the need for mutation of the genetic region of
545 interest. Finally, combining the current system with the expanding repertoire of Cas9-versions
546 and mutants (Knott & Doudna, 2018) should facilitate multiplex targeting and enquiry of
547 complex phenotypic behaviors. For example, in case of the specific phenotype we studied here,
548 targeting multiple kinetochore/Ctf19c subunits to adjacent loci should allow for more complete
549 reconstitution and interrogation of kinetochore-driven regulation of DSB suppression and
550 crossover repair control.
551

Acknowledgements

We thank the Vader and Bird (Max Planck Institute of Molecular Physiology, Dortmund, Germany) laboratories for ideas and helpful discussions. We thank Richard Cardoso da Silva (Max Planck Institute of Molecular Physiology, Dortmund, Germany) for mapping Spo11-oligo datasets. We acknowledge Andrea Musacchio (Max Planck Institute of Molecular Physiology, Dortmund, Germany) for ongoing support. We thank Stephen Hinshaw (Harvard Medical School, Boston, USA) for comments on the manuscript and for sharing illustrations depicting the structural organization of the budding yeast kinetochore. We thank John Weir (Friedrich Miescher Laboratory, Tübingen, Germany) and Vivek B. Raina (Max Planck Institute of Molecular Physiology, Dortmund, Germany) for comments on the manuscript. Work in the Vader laboratory was financially supported by the European Research Council (ERC Starting Grant URDNA, agreement nr. [638197], to G.V.) and the Max Planck Society. Work in the Marston laboratory was funded by a Wellcome Senior Research Fellowship [107827] and core funding for the Wellcome Centre for Cell biology [203149]. A.N.V. acknowledges support from INSPIRE, Department of Science and Technology (DST), Government of India, and from the Department of Biological Sciences, IISER Kolkata, India.

Author contribution

L-M.K., G.V., V.M and A.L.M. conceived and designed experiments. L-M.K., V.M., S.R., A.N.V, and G.V. performed experiments. G.V. and A.L.M. supervised the study. G.V. wrote the manuscript with input from all authors.

Figure legends

Figure 1. a dCas9/CRISPR-based targeting system. A. Schematic of dCas9-based fusion protein used in this study. Note that the 3xFlag moiety also functions as a peptide linker in between kinetochore factor of interest and dCas9. **B**. Schematic of fusion construct design. **C**. Western blot analysis of expression of 3xFlag-dCas9 during meiotic G2/prophase at defined hours after induction into the meiotic program. Pgk1 was used as a loading control. **D**. Schematic of live cell reporter assay on the right arm of Chromosome *VIII*. See Material and Methods for more information. **E**. Schematic of meiotic recombination, chromosome segregation and assortment of chromosomes in haploid gametes, yielding differentially fluorescent behaviors that report on recombination frequencies. **F**. Example of three tetrads from a meiotic culture with the described live cell reporter. Cells I. and II. are parental ditype, III. is tetratype. No rec.= no recombination, rec.=recombination. **G**. ChIP-qPCR (α-Flag ChIP) analysis of CEN3/Chr. *III*/Chr.*VIII* regions in yeast strains expressing 3xFlag-dCas9 in combination with sgRNA '*mock*', '*III*' and '*VIII*' during meiotic G2/prophase (5 hours). Primers pairs used for *CEN3:* GV2569/G2570, *III*: GV2464/GV2465, *VIII:* GV2472/GV2473. **H**. Map distances in centiMorgans (cM) and standard error determined for chromosomal arm interval as described in Materials and Methods and depicted in **D**. Data are from (Vincenten et al., 2015) and for 3xFlag-dCas9 in combination with sgRNAs '*mock*', '*III*' and '*VIII*', as indicated. p-values were obtained using Fisher's exact test (n.s. (non-significant) ≥0.05, * $p<0.05$; ** $p<0.0001$).

Figure 2. dCas9/CRISPR-based targeting reveals a role for Ctf19 in crossover control. A. Schematic of the budding yeast kinetochore, adapted from (Hinshaw & Harrison, 2019). The investigated kinetochore subcomplexes are highlighted. Individual factors that were used as dCas9-fusion are indicated in bold. **B.** Western blot analysis of expression of indicated

3xFLAG-dCas9 fusion constructs during meiotic G2/prophase (5 hours). Pgk1 was used as a loading control. **C.** Map distances in centiMorgans (cM) and standard error determined for chromosomal arm interval in cells expressing indicated 3xFLAG-dCas9 fusion constructs and '*VIII*' sgRNA. p-values were obtained using Fisher's exact test (n.s. (non-significant) ≥0.05, * p<0.05; ** p<0.0001). **D**. Map distances in centiMorgans (cM) and standard error determined for chromosomal arm interval in cells expressing indicated 3xFLAG-dCas9 fusion constructs and '*mock*', '*III*', or '*VIII*' sgRNAs. p-values were obtained using Fisher's exact test (n.s. (non-significant) ≥0.05, * p<0.05; ** p<0.0001).

Figure 3. Dissection of Ctf19-dependent crossover control. A. Schematic of the budding yeast kinetochore, adapted from (Hinshaw & Harrison, 2019), indicating effects of Ctf19-targeting on chromosome arm interval (*i.e*. co-targeting of binding partners and functional requirement). **B.** Co-immunoprecipitation of Ctf19-3xFlag-dCas9 and Mcm21-3HA (via α-Flag IP) during meiotic prophase (5 hours into meiotic program). Pgk1 and Histone H3 are used as loading control. **C**. ChIP-qPCR (α-HA ChIP) analysis of *CEN3*/Chr. *III*/Chr. *VIII* regions in yeast strains expressing indicated factors (5 hours). Primers pairs used for *CEN3:* GV2569/G2570, *III*: GV2464/GV2465, *VIII:* GV2472/GV2473. **D**. Co-immunoprecipitation of Ctf19-3xFlag-dCas9 and Chl4-6HA (via α-Flag IP) during meiotic prophase (5 hours into meiotic program). Pgk1 and Histone H3 are used as loading control. **E**. ChIP-qPCR (α-HA ChIP) analysis of *CEN3*/Chr. *III*/Chr. *VIII* regions in yeast strains expressing indicated factors (5 hours). Primers pairs used for *CEN3:* GV2569/G2570, *III*: GV2464/GV2465, *VIII:* GV2472/GV2473. **F**. Map distances in centiMorgans (cM) and standard error determined for chromosomal arm interval in *iml3Δ* cells expressing indicated 3xFLAG-dCas9 fusion constructs and '*VIII*' sgRNA. p-values were obtained using Fisher's exact test (n.s. (non-significant) ≥0.05, * p<0.05; ** p<0.0001). **G**. Western blot analysis of expression of indicated

623 3xFLAG-dCas9 fusion constructs in *iml3Δ* cells during meiotic G2/prophase (5 hours), as used
624 in **F**.

625 **Figure 4. Phosphorylation of the NH_2-terminus of Ctf19-dependent drives crossover**
626 **control. A.** Schematic of the budding yeast kinetochore, adapted from (Hinshaw & Harrison,
627 2019), indicating the molecular connection between DDK, the NH_2-terminus of Ctf19,
628 Scc2/Scc4 and cohesin function. **B**. Map distances in centiMorgans (cM) and standard error
629 determined for chromosomal arm interval in cells expressing indicated 3xFLAG-dCas9 fusion
630 constructs and '*VIII*' sgRNA. p-values were obtained using Fisher's exact test (n.s. (non-
631 significant) ≥0.05, * p<0.05; ** p<0.0001). **C.** Western blot analysis of expression of indicated
632 3xFLAG-dCas9 fusion constructs cells during meiotic G2/prophase (5 hours), as used in **B**. **D**.
633 Co-immunoprecipitation of Ctf19-3xFlag-dCas9, Ctf19-9A-3xFlag-dCas9and Mcm21-3HA
634 (via α-Flag IP) during meiotic prophase (5 hours into meiotic program). Pgk1 and Histone H3
635 are used as loading control. **E**. Schematic of $Ctf19_{1\text{-}30}$-3xFlag-dCas9. **F**. Map distances in
636 centiMorgans (cM) and standard error determined for chromosomal arm interval in cells
637 expressing indicated 3xFLAG-dCas9 fusion constructs and '*VIII*' sgRNA. p-values were
638 obtained using Fisher's exact test (n.s. (non-significant) ≥0.05, * p<0.05; ** p<0.0001). **G**.
639 Western blot analysis of expression of indicated 3xFLAG-dCas9 fusion constructs cells during
640 meiotic G2/prophase (5 hours), as used in **F**.

641 **Figure 5. Manipulating Ctf19-dependent crossover strength. A.** Schematic of the budding
642 yeast kinetochore, adapted from (Hinshaw & Harrison, 2019), indicating the 'dimeric' nature
643 of Ctf19c within the kinetochore, and the role of Ctf3 in DDK recruitment. **B**. Schematic of
644 $Ctf19_{1\text{-}30(2x)}$-3xFlag-dCas9. 6xG indicates 6xGlycine present between the two Ctf19 moieties.
645 **C**. Map distances in centiMorgans (cM) and standard error determined for chromosomal arm
646 interval in cells expressing indicated 3xFLAG-dCas9 fusion constructs and '*VIII*' sgRNA. p-

values were obtained using Fisher's exact test (n.s. (non-significant) ≥0.05, * p<0.05; ** p<0.0001). **D.** Western blot analysis of expression of indicated 3xFLAG-dCas9 fusion constructs cells during meiotic G2/prophase (5 hours), as used in **C**. **E**. Map distances in centiMorgans (cM) and standard error determined for chromosomal arm interval in cells expressing $Ctf19_{1\text{-}30(2x)}$-3xFlag-dCas9 and '*VIII*' sgRNA in *MCM21* or *mcm21Δ* cells. p-values were obtained using Fisher's exact test (n.s. (non-significant) ≥0.05, * p<0.05; ** p<0.0001). **F.** Western blot analysis of expression of $ctf19_{1\text{-}30(2x)}$-3xFlag-dCas9 in cells *MCM21* or *mcm21Δ* cells during meiotic G2/prophase (5 hours), as used in **E**. **G**. Schematic of Ctf19-3xFlag-dCas9-Dbf4. 6xG indicates 6xGlycine present between the dCas9 and Dbf4. **H**. Map distances in centiMorgans (cM) and standard error determined for chromosomal arm interval in cells expressing indicated 3xFLAG-dCas9 fusion constructs and '*VIII*' sgRNA. p-values were obtained using Fisher's exact test (n.s. (non-significant) ≥0.05, * p<0.05; ** p<0.0001). **I**. Western blot analysis of expression of indicated 3xFLAG-dCas9 fusion constructs cells during meiotic G2/prophase (5 hours), as used in **H**.

Figure 6. DSBs are not affected by dCas9-dependent targeting of Ctf19 fusions. A. Schematic of the genomic region around the '*YCR047C*' DSB hotspot on Chromosome *III*. SGD coordinates for binding of sgRNA '*III*' are indicated. Representative genome browser profile of meiotic hotspots for Spo11-oligo mapping (Zhu & Keeney, 2015). Normalized Spo11 oligo counts (RPM) is shown. **B.** Southern blot of YCR047C DSB hotspot, in yeast expressing the indicated dCas9 constructs and the sgRNA '*III*'. Time into the meiotic time course are indicated. Note that the *sae2Δ* background was used to prevent DSB resection and repair. **C**. Quantification of **B**. Error bars indicated standard error of the mean from three experiments.

Figure 7. The DDK-Ctf19-Scc2/4-cohesin pathway affects pericentromeric crossover suppression. A. Map distances in centiMorgans (cM) and standard error determined for a

671 pericentromeric (left panel) and chromosomal arm (right panel) intervals in wild type, *ctf19-9A*

672 and *ctf19Δ* cells. p-values were obtained using Fisher's exact test (n.s. (non-significant) ≥0.05,

673 * $p<0.05$; ** $p<0.0001$).

674

675 **References**

676 Blitzblau HG, Bell GW, Rodriguez J, Bell SP, Hochwagen A (2007) Mapping of meiotic single-
677 stranded DNA reveals double-stranded-break hotspots near centromeres and telomeres. *Current*
678 *biology : CB* 17: 2003-12
679 Borde V, Wu TC, Lichten M (1999) Use of a recombination reporter insert to define meiotic
680 recombination domains on chromosome III of Saccharomyces cerevisiae. *Molecular and*
681 *cellular biology* 19: 4832-42
682 Buhler C, Borde V, Lichten M (2007) Mapping meiotic single-strand DNA reveals a new
683 landscape of DNA double-strand breaks in Saccharomyces cerevisiae. *PLoS biology* 5: e324
684 Centola M, Carbon J (1994) Cloning and characterization of centromeric DNA from
685 Neurospora crassa. *Molecular and cellular biology* 14: 1510-9
686 Cheeseman IM, Desai A (2008) Molecular architecture of the kinetochore-microtubule
687 interface. *Nature reviews Molecular cell biology* 9: 33-46
688 Choi K (2017) Advances towards Controlling Meiotic Recombination for Plant Breeding. *Mol*
689 *Cells* 40: 814-822
690 Copenhaver GP, Nickel K, Kuromori T, Benito MI, Kaul S, Lin X, Bevan M, Murphy G, Harris
691 B, Parnell LD, McCombie WR, Martienssen RA, Marra M, Preuss D (1999) Genetic definition
692 and sequence analysis of Arabidopsis centromeres. *Science* 286: 2468-74
693 Davidson IF, Bauer B, Goetz D, Tang W, Wutz G, Peters JM (2019) DNA loop extrusion by
694 human cohesin. *Science* 366: 1338-1345
695 De Wulf P, McAinsh AD, Sorger PK (2003) Hierarchical assembly of the budding yeast
696 kinetochore from multiple subcomplexes. *Genes & development* 17: 2902-21
697 Ellermeier C, Higuchi EC, Phadnis N, Holm L, Geelhood JL, Thon G, Smith GR (2010) RNAi
698 and heterochromatin repress centromeric meiotic recombination. *Proceedings of the National*
699 *Academy of Sciences of the United States of America* 107: 8701-5
700 Fernius J, Marston AL (2009) Establishment of cohesion at the pericentromere by the Ctf19
701 kinetochore subcomplex and the replication fork-associated factor, Csm3. *PLoS genetics* 5:
702 e1000629
703 Fujita T, Yuno M, Fujii H (2018) An enChIP system for the analysis of bacterial genome
704 functions. *BMC Res Notes* 11: 387
705 Gascoigne KE, Takeuchi K, Suzuki A, Hori T, Fukagawa T, Cheeseman IM (2011) Induced
706 ectopic kinetochore assembly bypasses the requirement for CENP-A nucleosomes. *Cell* 145:
707 410-22
708 Gerton JL, DeRisi J, Shroff R, Lichten M, Brown PO, Petes TD (2000) Inaugural article: global
709 mapping of meiotic recombination hotspots and coldspots in the yeast Saccharomyces
710 cerevisiae. *Proceedings of the National Academy of Sciences of the United States of America*
711 97: 11383-90
712 Gilbert LA, Larson MH, Morsut L, Liu Z, Brar GA, Torres SE, Stern-Ginossar N, Brandman
713 O, Whitehead EH, Doudna JA, Lim WA, Weissman JS, Qi LS (2013) CRISPR-mediated
714 modular RNA-guided regulation of transcription in eukaryotes. *Cell* 154: 442-51
715 Gore MA, Chia JM, Elshire RJ, Sun Q, Ersoz ES, Hurwitz BL, Peiffer JA, McMullen MD,
716 Grills GS, Ross-Ibarra J, Ware DH, Buckler ES (2009) A first-generation haplotype map of
717 maize. *Science* 326: 1115-7
718 Gutierrez-Escribano P, Newton MD, Llauro A, Huber J, Tanasie L, Davy J, Aly I, Aramayo R,
719 Montoya A, Kramer H, Stigler J, Rueda DS, Aragon L (2019) A conserved ATP- and Scc2/4-
720 dependent activity for cohesin in tethering DNA molecules. *Sci Adv* 5: eaay6804
721 Hassold T, Hunt P (2001) To err (meiotically) is human: the genesis of human aneuploidy. *Nat*
722 *Rev Genet* 2: 280-91

723 Hinshaw SM, Harrison SC (2019) The structure of the Ctf19c/CCAN from budding yeast. *eLife*
724 8
725 Hinshaw SM, Makrantoni V, Harrison SC, Marston AL (2017) The Kinetochore Receptor for
726 the Cohesin Loading Complex. *Cell* 171: 72-84 e13
727 Hinshaw SM, Makrantoni V, Kerr A, Marston AL, Harrison SC (2015) Structural evidence for
728 Scc4-dependent localization of cohesin loading. *eLife* 4: e06057
729 Ho KH, Tsuchiya D, Oliger AC, Lacefield S (2014) Localization and function of budding yeast
730 CENP-A depends upon kinetochore protein interactions and is independent of canonical
731 centromere sequence. *Cell reports* 9: 2027-33
732 Hunter N (2015) Meiotic Recombination: The Essence of Heredity. *Cold Spring Harbor*
733 *perspectives in biology* 7
734 Keeney S (2001) Mechanism and control of meiotic recombination initiation. *Curr Top Dev*
735 *Biol* 52: 1-53
736 Kiermaier E, Woehrer S, Peng Y, Mechtler K, Westermann S (2009) A Dam1-based artificial
737 kinetochore is sufficient to promote chromosome segregation in budding yeast. *Nature cell*
738 *biology* 11: 1109-15
739 Kim KP, Weiner BM, Zhang L, Jordan A, Dekker J, Kleckner N (2010) Sister cohesion and
740 structural axis components mediate homolog bias of meiotic recombination. *Cell* 143: 924-37
741 Knott GJ, Doudna JA (2018) CRISPR-Cas guides the future of genetic engineering. *Science*
742 361: 866-869
743 Koehler KE, Hawley RS, Sherman S, Hassold T (1996) Recombination and nondisjunction in
744 humans and flies. *Hum Mol Genet* 5 Spec No: 1495-504
745 Kuhl LM, Vader G (2019) Kinetochores, cohesin, and DNA breaks: Controlling meiotic
746 recombination within pericentromeres. *Yeast* 36: 121-127
747 Lacefield S, Lau DT, Murray AW (2009) Recruiting a microtubule-binding complex to DNA
748 directs chromosome segregation in budding yeast. *Nature cell biology* 11: 1116-20
749 Lamb NE, Sherman SL, Hassold TJ (2005) Effect of meiotic recombination on the production
750 of aneuploid gametes in humans. *Cytogenet Genome Res* 111: 250-5
751 Lambie EJ, Roeder GS (1988) A yeast centromere acts in cis to inhibit meiotic gene conversion
752 of adjacent sequences. *Cell* 52: 863-73
753 Lambing C, Franklin FC, Wang CR (2017) Understanding and Manipulating Meiotic
754 Recombination in Plants. *Plant Physiol* 173: 1530-1542
755 Lang J, Barber A, Biggins S (2018) An assay for de novo kinetochore assembly reveals a key
756 role for the CENP-T pathway in budding yeast. *eLife* 7
757 Laughery MF, Hunter T, Brown A, Hoopes J, Ostbye T, Shumaker T, Wyrick JJ (2015) New
758 vectors for simple and streamlined CRISPR-Cas9 genome editing in Saccharomyces cerevisiae.
759 *Yeast* 32: 711-20
760 Liu X, Zhang Y, Chen Y, Li M, Zhou F, Li K, Cao H, Ni M, Liu Y, Gu Z, Dickerson KE, Xie
761 S, Hon GC, Xuan Z, Zhang MQ, Shao Z, Xu J (2017) In Situ Capture of Chromatin Interactions
762 by Biotinylated dCas9. *Cell* 170: 1028-1043 e19
763 Mahtani MM, Willard HF (1998) Physical and genetic mapping of the human X chromosome
764 centromere: repression of recombination. *Genome research* 8: 100-10
765 Murakami H, Keeney S (2014) Temporospatial coordination of meiotic DNA replication and
766 recombination via DDK recruitment to replisomes. *Cell* 158: 861-873
767 Musacchio A, Desai A (2017) A Molecular View of Kinetochore Assembly and Function.
768 *Biology (Basel)* 6
769 Nakaseko Y, Adachi Y, Funahashi S, Niwa O, Yanagida M (1986) Chromosome walking shows
770 a highly homologous repetitive sequence present in all the centromere regions of fission yeast.
771 *The EMBO journal* 5: 1011-21

772 Nambiar M, Smith GR (2018) Pericentromere-Specific Cohesin Complex Prevents Meiotic
773 Pericentric DNA Double-Strand Breaks and Lethal Crossovers. *Molecular cell* 71: 540-553 e4
774 Paldi F., Alver B., Robertson D., Schalbetter S.A., Kerr A., Kelly D.A., Neale M.J., Baxter J.,
775 Marston A.L. (2019) Convergent genes shape budding yeast pericentromeres. *BioRxiv*
776 Pan J, Sasaki M, Kniewel R, Murakami H, Blitzblau HG, Tischfield SE, Zhu X, Neale MJ,
777 Jasin M, Socci ND, Hochwagen A, Keeney S (2011) A hierarchical combination of factors
778 shapes the genome-wide topography of yeast meiotic recombination initiation. *Cell* 144: 719-
779 31
780 Pekgoz Altunkaya G, Malvezzi F, Demianova Z, Zimniak T, Litos G, Weissmann F, Mechtler
781 K, Herzog F, Westermann S (2016) CCAN Assembly Configures Composite Binding
782 Interfaces to Promote Cross-Linking of Ndc80 Complexes at the Kinetochore. *Current biology*
783 *: CB* 26: 2370-8
784 Petela NJ, Gligoris TG, Metson J, Lee BG, Voulgaris M, Hu B, Kikuchi S, Chapard C, Chen
785 W, Rajendra E, Srinivisan M, Yu H, Lowe J, Nasmyth KA (2018) Scc2 Is a Potent Activator
786 of Cohesin's ATPase that Promotes Loading by Binding Scc1 without Pds5. *Molecular cell* 70:
787 1134-1148 e7
788 Petronczki M, Siomos MF, Nasmyth K (2003) Un menage a quatre: the molecular biology of
789 chromosome segregation in meiosis. *Cell* 112: 423-40
790 Pot I, Measday V, Snydsman B, Cagney G, Fields S, Davis TN, Muller EG, Hieter P (2003)
791 Chl4p and iml3p are two new members of the budding yeast outer kinetochore. *Molecular*
792 *biology of the cell* 14: 460-76
793 Puechberty J, Laurent AM, Gimenez S, Billault A, Brun-Laurent ME, Calenda A, Marcais B,
794 Prades C, Ioannou P, Yurov Y, Roizes G (1999) Genetic and physical analyses of the
795 centromeric and pericentromeric regions of human chromosome 5: recombination across 5cen.
796 *Genomics* 56: 274-87
797 Rockmill B, Voelkel-Meiman K, Roeder GS (2006) Centromere-proximal crossovers are
798 associated with precocious separation of sister chromatids during meiosis in Saccharomyces
799 cerevisiae. *Genetics* 174: 1745-54
800 Saintenac C, Falque M, Martin OC, Paux E, Feuillet C, Sourdille P (2009) Detailed
801 recombination studies along chromosome 3B provide new insights on crossover distribution in
802 wheat (Triticum aestivum L.). *Genetics* 181: 393-403
803 Sasaki M, Lange J, Keeney S (2010) Genome destabilization by homologous recombination in
804 the germ line. *Nature reviews Molecular cell biology* 11: 182-95
805 Schleiffer A, Maier M, Litos G, Lampert F, Hornung P, Mechtler K, Westermann S (2012)
806 CENP-T proteins are conserved centromere receptors of the Ndc80 complex. *Nature cell*
807 *biology* 14: 604-13
808 Schmitzberger F, Harrison SC (2012) RWD domain: a recurring module in kinetochore
809 architecture shown by a Ctf19-Mcm21 complex structure. *EMBO Rep* 13: 216-22
810 Schmitzberger F, Richter MM, Gordiyenko Y, Robinson CV, Dadlez M, Westermann S (2017)
811 Molecular basis for inner kinetochore configuration through RWD domain-peptide interactions.
812 *The EMBO journal* 36: 3458-3482
813 Takahashi TS, Basu A, Bermudez V, Hurwitz J, Walter JC (2008) Cdc7-Drf1 kinase links
814 chromosome cohesion to the initiation of DNA replication in Xenopus egg extracts. *Genes &*
815 *development* 22: 1894-905
816 Thacker D, Lam I, Knop M, Keeney S (2011) Exploiting spore-autonomous fluorescent protein
817 expression to quantify meiotic chromosome behaviors in Saccharomyces cerevisiae. *Genetics*
818 189: 423-39
819 Vader G, Blitzblau HG, Tame MA, Falk JE, Curtin L, Hochwagen A (2011) Protection of
820 repetitive DNA borders from self-induced meiotic instability. *Nature* 477: 115-9

821 Vershon AK, Hollingsworth NM, Johnson AD (1992) Meiotic induction of the yeast HOP1
822 gene is controlled by positive and negative regulatory sites. *Molecular and cellular biology* 12:
823 3706-14
824 Vincenten N, Kuhl LM, Lam I, Oke A, Kerr AR, Hochwagen A, Fung J, Keeney S, Vader G,
825 Marston AL (2015) The kinetochore prevents centromere-proximal crossover recombination
826 during meiosis. *eLife* 4
827 Wang H, La Russa M, Qi LS (2016) CRISPR/Cas9 in Genome Editing and Beyond. *Annu Rev*
828 *Biochem* 85: 227-64
829 Westphal T, Reuter G (2002) Recombinogenic effects of suppressors of position-effect
830 variegation in Drosophila. *Genetics* 160: 609-21
831 Xu X, Tao Y, Gao X, Zhang L, Li X, Zou W, Ruan K, Wang F, Xu GL, Hu R (2016) A CRISPR-
832 based approach for targeted DNA demethylation. *Cell Discov* 2: 16009
833 Yan K, Yang J, Zhang Z, McLaughlin SH, Chang L, Fasci D, Ehrenhofer-Murray AE, Heck
834 AJR, Barford D (2019) Structure of the inner kinetochore CCAN complex assembled onto a
835 centromeric nucleosome. *Nature* 574: 278-282
836 Zhu X, Keeney S (2015) High-Resolution Global Analysis of the Influences of Bas1 and Ino4
837 Transcription Factors on Meiotic DNA Break Distributions in Saccharomyces cerevisiae.
838 *Genetics* 201: 525-42

839

Figure 1

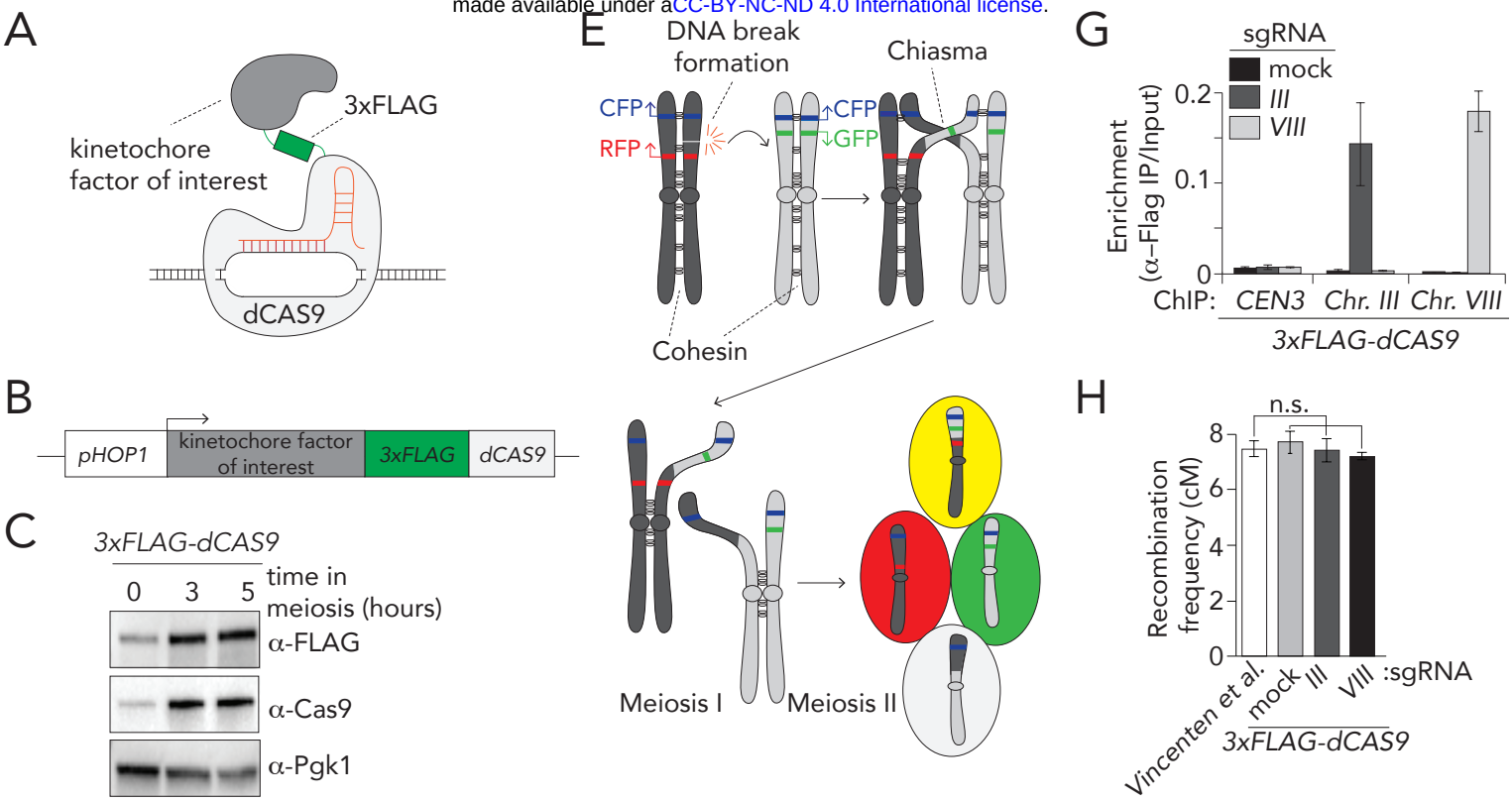

Figure 2

A

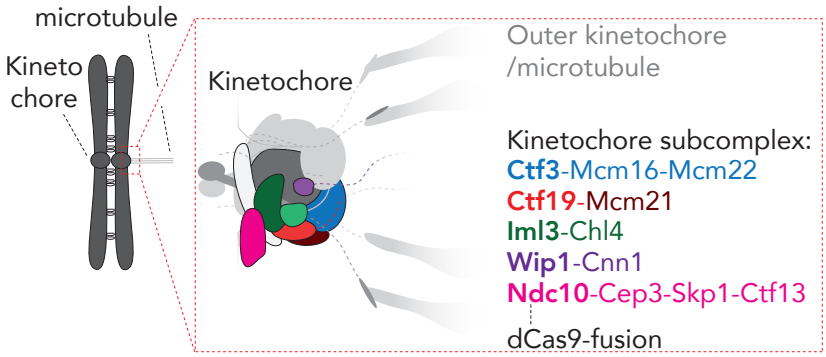

B

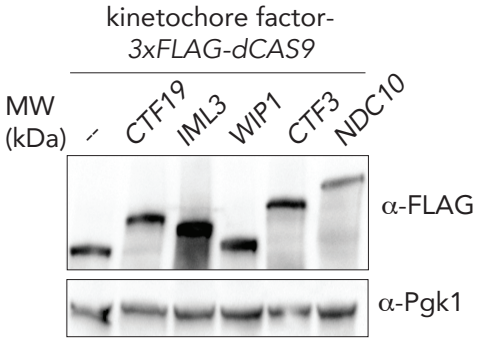

C

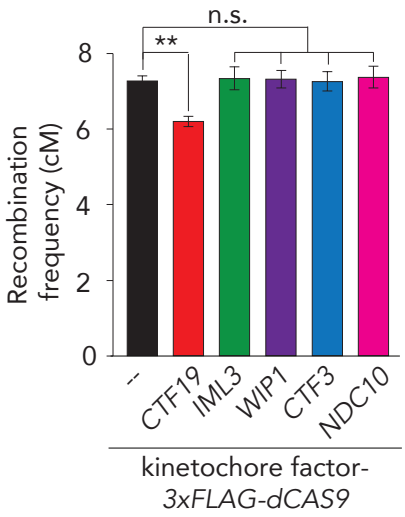

D

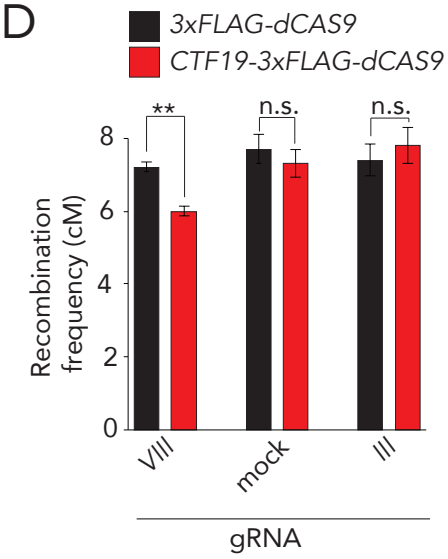

Figure 3

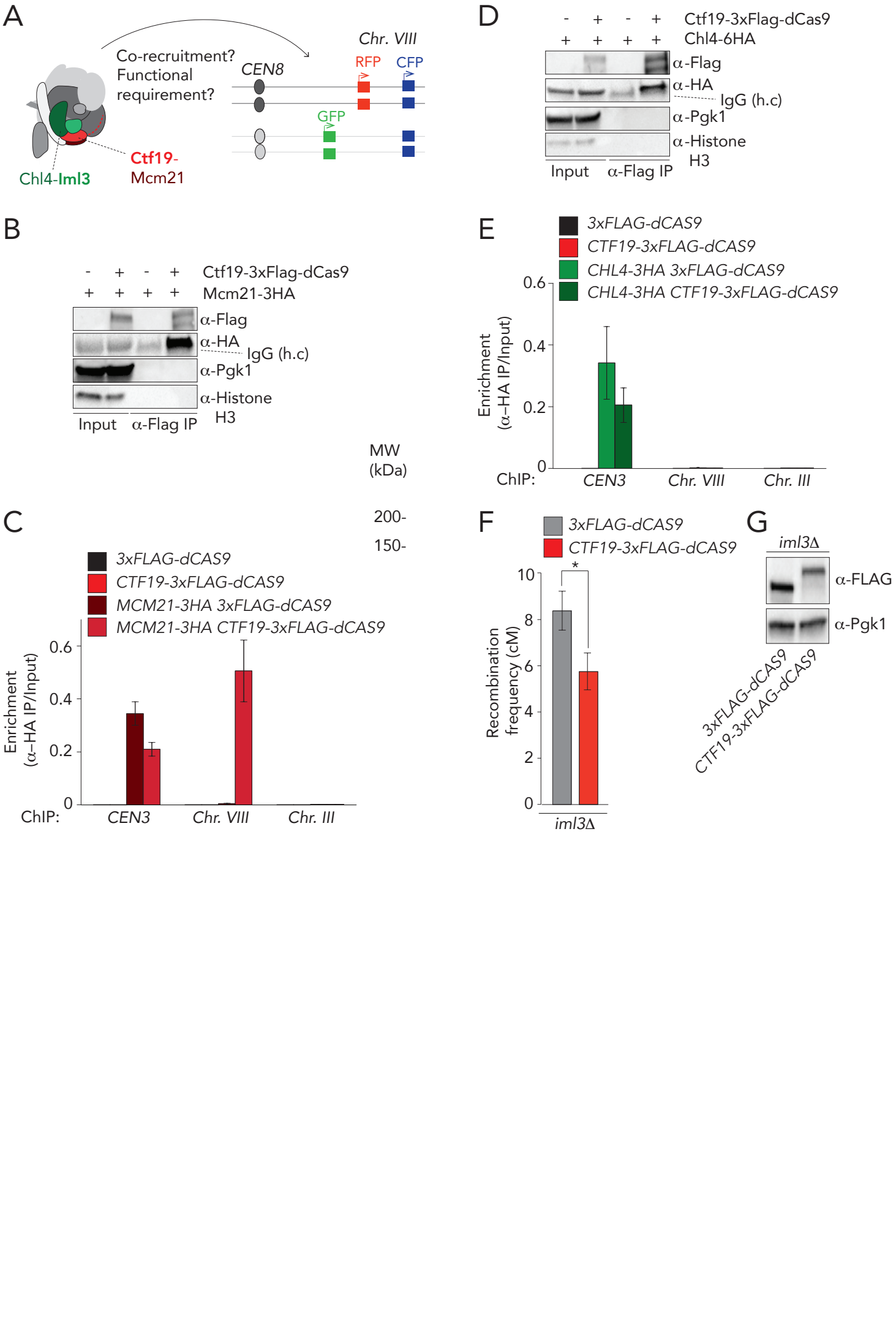

Figure 4

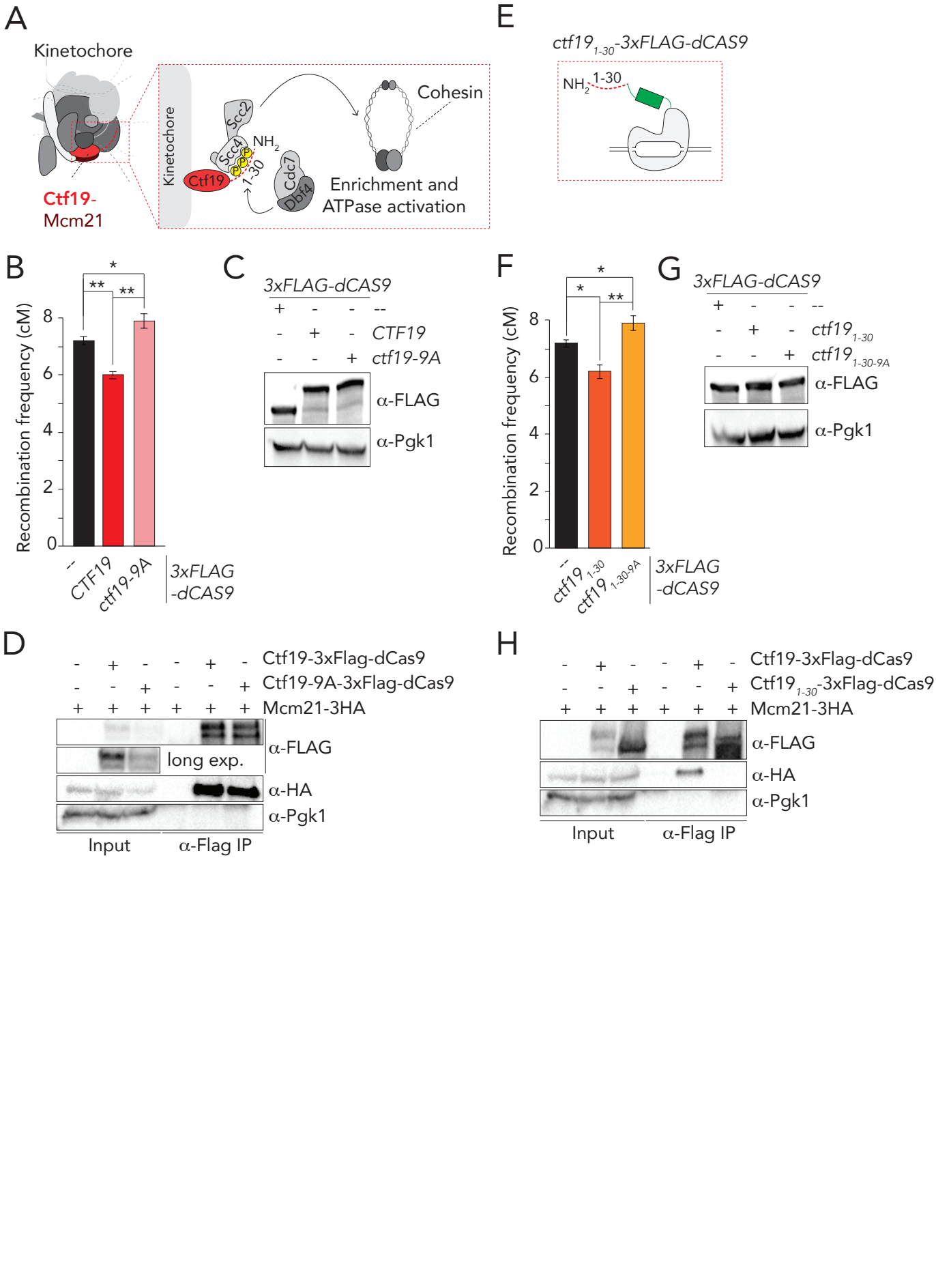

Figure 5

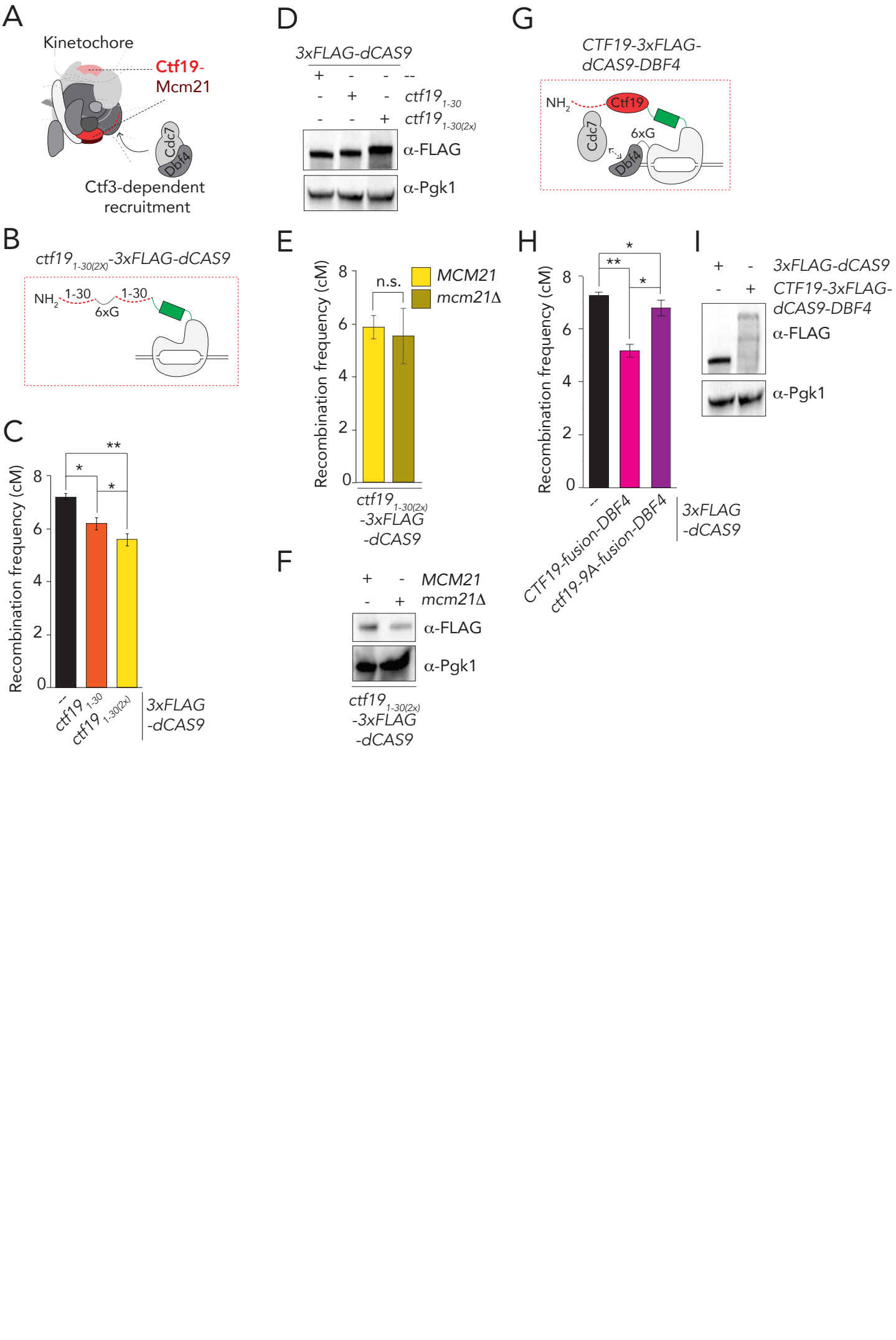

Figure 6

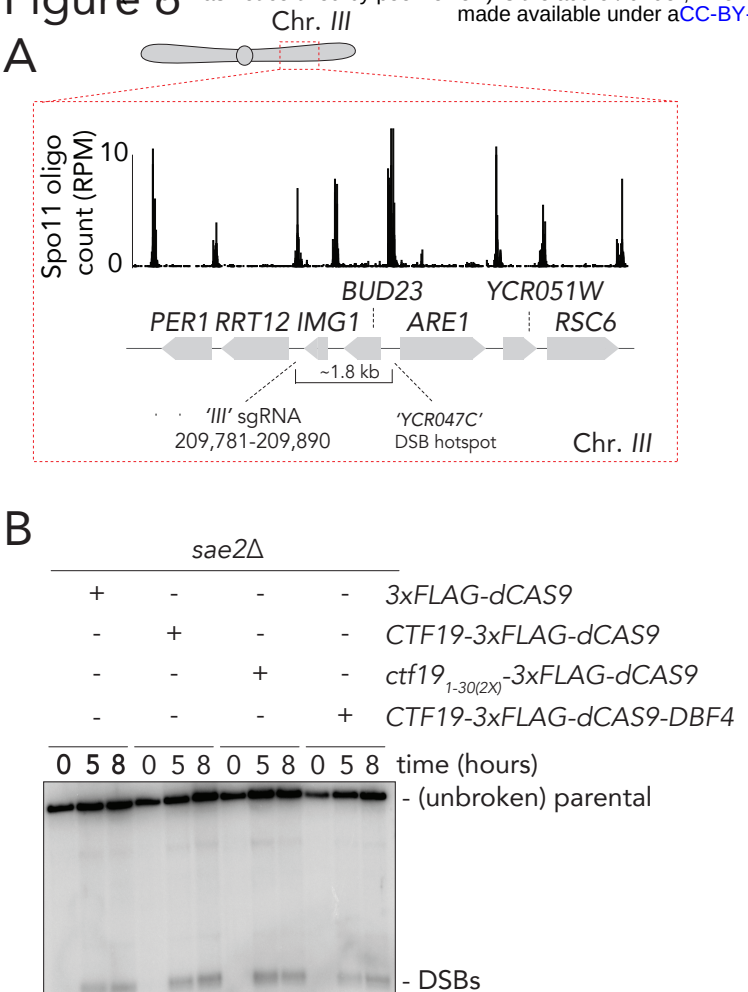

Figure 7

A